Synthesis and Structural Characterization of $[Mn(ethyl\ isonicotinate)_2(N_3)_2]_n$, a Two-Dimensional Alternating Ferromagnetic−Antiferromagnetic Compound. Magnetostructural Correlations for the End-to-End Pseudohalide−Manganese System

Albert Escuer,*,† Ramon Vicente,† Mohamed A. S. Goher,*,‡,§ and Franz A. Mautner⊥

Departament de Química Inorgànica, Universitat de Barcelona, Diagonal 647, 08028 Barcelona, Spain, Department of Chemistry, Faculty of Science, Alexandria University, Alexandria 21321, Egypt, and Institut für Physikalische und Theoretische Chemie, Technische Universität Graz, A-8010 Graz, Austria

Received March 29, 1996[⊗]

Three compounds with formula $[Mn(L)_2(N_3)_2]_n$, in which L is 4-acpy = 4-acetylpyridine (**1**), Etinc = ethyl isonicotinate (**2**), and py = pyridine (**3**), have been studied from the magnetic point of view. The new compound $[Mn(L)_2(N_3)_2]_n$ (**2**) crystallizes in the monoclinic system, space group $P2_1/a$ (No. 14), formula $[C_{16}H_{18}MnN_8O_4]$, with $a = 15.176(5)$ Å, $b = 9.060(3)$ Å, $c = 15.760(6)$ Å, $\beta = 111.62(3)°$, and $Z = 4$. Compounds **1** and **2** are two-dimensional systems, whereas **3** is a 3-D compound. Compound **2** shows ferromagnetic $Mn_2(N_3)_2$ dimeric entities linked antiferromagnetically to the four neighboring dimeric entities by four end-to-end azido bridges, leading to an alternate ferromagnetic−antiferromagnetic two-dimensional compound. MO calculations have been performed to study the superexchange pathway for the manganese 1,3-azido system.

Introduction

The number of first row polynuclear complexes in which the paramagnetic centers (copper[1] and nickel[2]) are linked by means of an azido ligand has markedly increased in the past few years. The interest of magnetochemists in this ligand is due to two main reasons: the magnetic behavior of the azido systems changes with the coordination mode of the ligand (end-to-end coordination gave from moderate to very strong antiferromagnetic coupling and end-on coordination generally gave ferromagnetic coupling), and the nuclearity of the polynuclear compounds is frequently greater than 2. From these properties, azido ligand complexes have been the object of studies on the superexchange pathway for the two coordination modes[1,3,4] and several homogeneous 1D antiferromagnets have also been characterized,[4,5] giving good examples of the behavior of this kind of system at low temperatures for exotic effects such as the Haldane gap phenomenon.[6] Combination of the two properties in extended nickel systems has recently allowed new magnetic systems such as alternating ferromagnetic−antiferromagnetic chains or planes.[7]

The manganese−azido system has been poorly explored to date, but the few reported compounds show a great variety of dimensionality and magnetic behaviors. Goher and Mautner have reported the monomeric[8] compound $[Mn(quin)(N_3)(H_2O)]\cdot H_2O$ (quin = quinaldinic acid), the complex $[NaMn(pyz)(N_3)_2(H_2O)_2]$ (pyz = 2-pyrazinic acid), which is the first structurally characterized 1,1-azido dinuclear manganese compound,[9] and the two-dimensional[10] $[Mn(pic)(N_3)(H_2O)]_n$ (pic = picolinic acid), which contains carboxylato−manganese Mn_2O_2 units linked to the four neighboring Mn_2O_2 units by means of four end-to-end azido bridges; the same authors have reported the three-dimensional[11] $[Mn(py)_2(N_3)_2]_n$ system. For all of them, only structural data without magnetic studies have been published. More recently, Rojo *et al*. reported the structural and magnetic characterization of the dimeric[12] $(\mu_{1,1}\text{-}N_3)_2[Mn(terpy)_2]_2(X)_2$ (terpy = terpyridine) and the ferromagnetic−antiferromagnetic alternating chain[13] $[Mn(bpy)(N_3)_2]_n$ (bpy = bipyridine), which show simultaneous end-to-end and end-on azido bridges.

In this work we study the compounds $[Mn(4\text{-}acpy)_2(N_3)_2]_n$ (**1**, acpy = 4-acetylpyridine), $[Mn(Etinc)_2(N_3)_2]_n$ (**2**, Etinc =

† Universitat de Barcelona.
‡ Alexandria University.
§ Present address: Chemistry Department, Faculty of Science, Kuwait University, P. O. Box 5969 Safat, 13060 Kuwait.
⊥ Technische Universität Graz.
⊗ Abstract published in *Advance ACS Abstracts,* September 15, 1996.

(1) Thompson, L. K.; Tandon, S. S.; Manuel, M. E. *Inorg. Chem.* **1995**, *34*, 2356, and references cited therein.
(2) Escuer, A.; Vicente, R.; Ribas, J.; Solans, X. *Inorg. Chem.* **1995**, *34*, 1793, and references cited therein.
(3) End-on mode: Sikorav, S.; Bkouche-Waksman, I.; Kahn, O. *Inorg. Chem.* **1984**, *23*, 490. Comarmond, J.; Plumeré, P.; Lehn, J. M.; Agnus, Y.; Louis, R.; Weiss, R.; Kahn, O.; Morgenstern-Badarau. *J. Am. Chem. Soc*. **1982**, *104*, 6330. Charlot, M. F.; Kahn, O.; Chaillet, M.; Larrieu, C. *J. Am. Chem. Soc*. **1986**, *24*, 2574.
(4) End-to-end mode: Escuer, A.; Vicente, R.; Ribas, J.; El Fallah, M. S.; Solans, X.; Font-Bardia, M. *Inorg. Chem*. **1993**, *32*, 3727. Escuer, A.; Vicente, R.; Ribas, J.; El Fallah, M. S.; Solans, X.; Font-Bardia, M. *Inorg. Chem*. **1994**, *33*, 1842. Ribas, J.; Monfort, M.; Bastos, C.; Diaz, C.; Solans, X. *Inorg. Chem.* **1993**, *32*, 3557. Vicente, R.; Escuer, A. *Polyhedron* **1995**, *14*, 2133. Escuer, A.; Vicente, R.; El Fallah, M. S.; Solans, X.; Font-Bardia, M. *J. Chem. Soc., Dalton Trans*. **1996**, 1013.
(5) Ribas, J.; Monfort, M.; Diaz, C.; Bastos, C.; Solans, X. *Inorg. Chem*. **1994**, *33*, 484. Cortés, R.; Urtiaga, K.; Lezama, L.; Pizarro, J. L.; Goñi, A.; Arriortua, M. I.; Rojo, T. *Inorg. Chem*. **1994**, *33*, 4009. Ribas, J.; Monfort, M.; Diaz, C.; Bastos, C.; Mer, C.; Solans, X. *Inorg. Chem*. **1995**, *34*, 4986.
(6) Takeuchi, T.; Yosida, T.; Inoue, K.; Yamashita, M.; Kumada, T.; Kindo.; Merah, S.; Verdaguer, M.; Renard. *J. Magn. Magn. Mater*. **1995**, *140*, 1633.
(7) Ribas, J.; Monfort, M.; Ghosh, B. K.; Solans, X. *Angew. Chem., Int. Ed. Engl*. **1994**, *33*, 2087. Ribas, J.; Monfort, M.; Solans, X.; Drillon, M. *Inorg. Chem*. **1994**, *33*, 742. Ribas, J.; Monfort, M.; Ghosh, B. K.; Solans, X.; Font-Bardia, M. *J. Chem. Soc., Chem. Commun*. **1995**, 2375.
(8) Goher, M. A. S.; Abu-Youssef, M. A. M.; Mautner, F. A.; Popitsch, A. *Polyhedron* **1993**, *12*, 1751.
(9) Goher, M. A. S.; Mautner, F. A.; Popitsch, A. *Polyhedron* **1993**, *12*, 2557.
(10) Goher, M. A. S.; Abu-Youssef, M. A. M.; Mautner, F. A.; Popitsch, A. *Polyhedron* **1992**, *11*, 2137.
(11) Goher, M. A. S.; Mautner, F. A. *Croat. Chem. Acta* **1990**, *63*, 559.
(12) Cortés, R.; Pizarro, L.; Lezama, L.; Arriortua, M. S.; Rojo, T. *Inorg. Chem*. **1994**, *33*, 2697.
(13) Cortés, R.; Lezama, L.; Pizarro, J. L.; Arriortua, M. I.; Solans, X.; Rojo, T. *Angew. Chem., Int. Ed. Engl*. **1994**, *33*, 2488.

S0020-1669(96)00346-1 CCC: $12.00

Table 1. Crystal Data for $[Mn(Etinc)_2(N_3)_2]$ (**2**)

chem formula	$[C_{16}H_{18}MnN_8O_4]$	V, Å^3	2014(1)
formula weight	441.31	Z	4
space group	$P2_1/a$ (No. 14)	T, C	20(2)
a, Å	15.176(5)	λ(Mo Kα), Å	0.710 69
b, Å	9.060(3)	d_{calc}, g·cm^{-3}	1.455
c, Å	15.760(6)	μ(Mo Kα), mm^{-1}	0.67
α, deg	90.00	R[a]	0.047
β, deg	111.62(3)	R_w[b]	0.045
γ, deg	90.00		

[a] $R(F_o) = \Sigma\{|F_o| - |F_c|\}/\Sigma F_o$. [b] $R_w(F_o) = [w\Sigma(|F_o| - |F_c|)^2/\Sigma wF_o^2]^{1/2}$.

ethyl isonicotinate), and for comparative purposes some structural and magnetic properties of $[Mn(py)_2(N_3)_2]_n$ (**3**, py = pyridine). Syntheses and some magnetic properties of **1** were reported as a preliminary communication.[14] Compound **1** was found to be a Heisenberg two-dimensional antiferromagnet, compound **2** is an alternating ferromagnetic−antiferromagnetic two-dimensional system, and **3** is a three-dimensional antiferromagnet.

EPR and susceptibility measurements show that compound **1** has 3D magnetic order below 28 K. Systems of this kind may be studied from two very different points of view: the ordered low-temperature phase and the paramagnetic high-temperature region. Our interest is focused on the latter magnetic properties, *i.e.*, the superexchange pathway for the end-to-end azido−manganese system. We have explored the factors that influence the coupling by MO extended-Huckel calculations, and the results were compared with those obtained for the nickel(II)−azido system.

Experimental Section

Synthesis. Compounds **1** and **3** were synthesized following published methods.[11,14] Compound **2** was prepared as follows: 5 mL of a water solution of sodium azide (0.42 g, 6.5 mmol) was dropwise added to a mixture of 10 mL of a water solution of manganese chloride trihydrate (0.591 g, 3mmol) and 20 mL of ethanolic solution of ethyl isonicotinate (1.5 g, 10 mmol). The final clear solution was kept in a refrigerator for 2 or 3 days to produce the complex as well-formed yellow crystals. Anal. Found (% (calcd (%)): C, 43.6 (43.55); H, 4.1 (4.10); N, 25.4 (25.38); Mn, 12.4 (12.24). IR spectra: in addition to the characteristic bands of the corresponding pyridyl derivatives, a very intense band due to the ν_{as} of the azido groups appears close to 2080 cm^{-1} for compounds **1** and **3**, whereas compound **2** shows a more complicated pattern with three signals at 2112, 2085, and 2058 cm^{-1}.

Spectral and Magnetic Measurements. Infrared spectra (400−4000 cm^{-1}) were recorded from KBr pellets on a Nicolet 520 FTIR spectrophotometer. Magnetic measurements were carried out with a Faraday type magnetometer (MANICS DSM8) equipped with an Oxford CF 1200 S helium continuous-flow cryostat working in the temperature range 300-4 K. The magnetic field was 1.5 T approximately; this magnetic field is correct for studying the paramagnetic region, but not for the ordered phase, out of the range of this work, for which low-field measurements are needed. Diamagnetic corrections were estimated from Pascal tables. EPR spectra were recorded with a Bruker ES200 spectrometer at X-band frequency equipped with an Oxford liquid-helium cryostat for variable temperature work.

Crystallographic Data Collection and Refinement of the Structures. $[Mn(4\text{-acpy})_2(N_3)_2]$ (1). Crystallographic data and details about the structure determination were previously reported in a preliminary communication.[14]

$[Mn(Etinc)_2(N_3)_2]$ (2). A piece of a transparent yellow crystal (approximate size: 0.45 × 0.35 × 0.23 mm) was selected and mounted on a modified STOE four-circle diffractometer. The crystallographic data, conditions retained for the intensity data collection, and some features of the structure refinement are listed in Table 1. The accurate unit-cell parameters were determined from automatic centering of 29 reflections (8° < θ < 14°) and refined by least-squares methods. Intensities were collected with graphite-monochromated Mo Kα radiation, using the ω-scan technique. For the compound **2**, 5067 reflections were collected in the range 5° < 2θ < 55° (±h, +k, +l), and 1859 reflections were assumed as observed by applying the condition $F > 3\sigma(F_o)$. Two reflections (111; 003) were collected every hour and used for intensity correction (intensity of the two standard reflections dropped continuously during data collection by 44%). Corrections were applied for Lorentz−polarization effects, for intensity decay, and for absorption (transmission factors: 0.934−1.000) using the DIFABS computer program.[15] The structure was solved by Patterson synthesis using the SHELXS[16] computer program, and refined by full-matrix least-squares methods, using the SHELX[17] computer program. The function minimized was $\Sigma\omega[|F_o| - |F_c|]^2$, where $\omega = 0.4955/(\sigma^2|F_o| + k|F_o|^2)$ ($k = 0.0$). f, f', and f'' were taken from ref 18. Hydrogen atoms were located on calculated positions and assigned with six common isotropic temperature factors (separate U(iso) values for each type of hydrogen in each Etinc molecule). The final R factor was 0.047 ($R_w = 0.045$) for all observed reflections. The number of parameters refined was 268. Maximum shift/esd = 0.05. Maximum and minimum peaks in the final difference synthesis were 0.30 and −0.32 e Å^{-3}, respectively. Final atomic coordinates and significant bond parameters are given in Tables 2 and 3, respectively.

Table 2. Atomic Coordinates (×10^4) and Equivalent Isotropic Displacement Parameters (Å^2 × 10^3) for $[Mn(Etinc)_2(N_3)_2]$ (**2**)

	X/a	Y/b	Z/c	U(eq)[a]
Mn(1)	1130(0)	4915(1)	4954(1)	38(0)
N(11)	1714(3)	3402(5)	4213(4)	75(4)
N(12)	2188(3)	2380(5)	4344(3)	50(3)
N(13)	2355(3)	1323(6)	4445(4)	84(4)
N(21)	−255(3)	3739(4)	4479(3)	43(3)
N(22)	−442(3)	2591(6)	4139(4)	66(4)
N(23)	−633(5)	1458(7)	3822(6)	178(9)
N(1)	1758(3)	3466(5)	6231(3)	46(3)
C(1)	2267(4)	4089(6)	7028(4)	57(4)
C(2)	2792(4)	3281(6)	7767(4)	57(4)
C(3)	2813(3)	1765(6)	7711(4)	44(4)
C(4)	2269(3)	1111(6)	6905(3)	46(4)
C(5)	1750(3)	1998(6)	6184(4)	47(4)
C(6)	3424(4)	911(7)	8517(4)	53(4)
O(1)	3889(3)	1460(5)	9229(3)	86(3)
O(2)	3430(2)	−499(4)	8323(3)	58(3)
C(7)	4065(4)	−1416(7)	9042(4)	71(5)
C(8)	3986(4)	−2944(7)	8623(5)	93(6)
N(2)	623(3)	6340(5)	3671(3)	42(3)
C(9)	637(3)	7801(6)	3714(4)	50(4)
C(10)	149(3)	8682(6)	2981(4)	50(4)
C(11)	−382(3)	8024(6)	2164(4)	47(4)
C(12)	−367(4)	6498(6)	2114(4)	55(4)
C(13)	143(3)	5705(6)	2874(4)	53(4)
C(14)	−977(4)	8887(7)	1360(5)	60(4)
O(3)	−1454(4)	8329(5)	645(3)	115(5)
O(4)	−969(3)	10293(4)	1512(3)	69(3)
C(15)	−1574(4)	11234(7)	787(4)	74(5)
C(16)	−1526(4)	12723(7)	1227(5)	88(6)

[a] U(eq) is defined as one-third of the trace of the orthogonalized $\mathbf{U}_{ij}$ tensor.

Results and Discussion

Description of the Structures. $[Mn(4\text{-acpy})_2(N_3)_2]_n$ (1). The structure of **1** consists of 2D manganese−azido sheets. Each manganese atom is placed in a centrosymmetrical octahedral environment. The coordination polyhedron is formed by two 4-acetylpyridine and four azido ligands coordinated in *trans*

(14) Escuer, A.; Vicente, R.; Goher, M. A. S.; Mautner, F. A. *Inorg. Chem.* **1995**, *34*, 5707.
(15) Walker, N.; Stuart, D. *Acta Crystallogr.* **1983**, *A39*, 158.
(16) Sheldrick, G. M. *Acta Crystallogr.* **1990**, *A46*, 467.
(17) Sheldrick, G. M. *SHELX. A computer program for crystal structure determination*; Univeristy of Cambridge: Cambridge, England, 1976.
(18) *International Tables for X-ray Crystallography*; Kynoch Press: Birmingham, England, 1974; Vol. IV, pp 99−110, 149.

Table 3. Selected Bond Lengths (Å) and Angles for $[Mn(Etinc)_2(N_3)_2]_n$ (**2**)

Manganese Environment			
Mn(1)−N(1)	2.295(5)	Mn(1)−N(21)	2.226(4)
Mn(1)−N(2)	2.281(5)	Mn(1)−N(13b)	2.164(5)
Mn(1)−N(11)	2.189(5)	Mn(1)−N(21c)	2.218(4)
N(1)−Mn(1)−N(2)	175.2(2)	N(21)−Mn(1)−N(13b)	169.1(2)
N(1)−Mn(1)−N(11)	89.4(2)	N(21)−Mn(1)−N(21c)	76.6(2)
N(1)−Mn(1)−N(21)	93.2(2)	Mn(1)−N(11)−N(12)	139.7(4)
N(1)−Mn(1)−N(13b)	86.6(2)	N(12)−N(13)−Mn(1a)	157.2(5)
N(1)−Mn(1)−N(21c)	94.5(2)	Mn(1)−N(21)−Mn(1c)	103.4(2)
N(2)−Mn(1)−N(11)	87.2(2)	Mn(1)−N(21)−N(22)	128.8(4)
N(2)−Mn(1)−N(21)	90.3(2)	N(22)−N(21)−Mn(1c)	126.9(4)
N(2)−Mn(1)−N(13b)	90.5(2)	Mn(1)−N(1)−C(1)	119.6(3)
N(2)−Mn(1)−N(21c)	89.4(2)	Mn(1)−N(1)−C(5)	122.0(4)
N(11)−Mn(1)−N(21)	92.2(2)	Mn(1)−N(2)−C(9)	121.7(4)
N(11)−Mn(1)−N(13b)	98.7(2)	Mn(1)−N(2)−C(13)	118.8(4)
N(11)−Mn(1)−N(21c)	168.3(2)		
Azido Ligands			
N(11)−N(12)	1.144(7)	N(21)−N(22)	1.157(7)
N(12)−N(13)	1.158(7)	N(22)−N(23)	1.132(9)
N(11)−N(12)−N(13)	177.5(6)	N(21)−N(22)−N(23)	178.3(7)

arrangement, elongated along the axis defined by the pyridyl ligands, Mn−N(1) = 2.291(3), Mn−N(11) = 2.192(3), and Mn−N(13) = 2.214(3) Å. Each azido ligand acts as a bridge with the next manganese atom in the end-to-end coordination mode, Mn−N(11)−N(12) = 151.6(2)°, Mn−N(13)−N(12b) = 129.0(2)°, and Mn−azido−Mn torsion angle, defined as the dihedral angle between the Mn−N(11)−N(12) and N(12)−N(13c)−Mn′ = 79.6°. As a consequence of these asymmetric bond angles and the torsion Mn−N_3−Mn angle, the planes defined by the manganese atom and the four N-(azido) atoms show a dihedral angle of 83.3°. The minimum Mn−Mn interplane distance is 11.563(5) Å. The structure of **1** is similar in its general trends to the $[Mn(EtOH)_2(SCN)_2]_n$ two-dimensional compound showing the most significant differences in the more asymmetric manganese−pseudohalide bond angles Mn−N−C = 169.0(1)° and Mn−S−C = 103.6(1)°.[19]

$[Mn(Etinc)_2(N_3)_2]_n$ (2). The structure also consists of a 2D manganese−azido compound, with each manganese in *trans* octahedral environment, bonded to four azido ligands and two axial pyridyl−(ethyl isonicotinate) ligands. A labeled schema is shown in Figure 1. In **2**, the four azido bridges show the two coordination modes: two azido ligands are coordinated in the end-on mode between two manganese atoms, giving a planar and centrosymmetric Mn_2N_2 unit. Each Mn_2N_2 fragment is linked to the four neighboring Mn_2N_2 units by means of four end-to-end azido bridges. Then, the structure of **2** is related to compound **1**, but holding dinuclear Mn_2N_2 units instead of single manganese atoms in $[Mn(4\text{-acpy})_2(N_3)_2]$, as is shown in Figure 2. Bond parameters in the end-on units show normal values for this kind of unit: Mn(1)−N(21) = 2.226(4) Å, Mn(1)−N(21c) = 2.218(4) Å, Mn(1)−N(21)−Mn(1c) = 103.4(2)°, N(21)−Mn(1)−N(21c) = 76.6(2)°. End-to-end azido bridges are strongly asymmetrical: Mn(1)−N(11)−N(12) = 139.7(4)°, Mn(1a)−N(13)−N(12) = 157.2(5)°. The dihedral angle Mn−N_3−Mn defined as the angle between the planes Mn(1)−N(11)−N(12) and N(12)−N(13)−Mn(1a) is 55.3(10)°, and the acute angle between neighboring Mn_2N_2 units is 67.49(17)°. The intersheet Mn−Mn distance is close to 15 Å for several manganese atoms.

It is interesting to compare these structures with the previously reported $[Mn(py)_2(N_3)_2]_n$ complex **3**, which shows the same

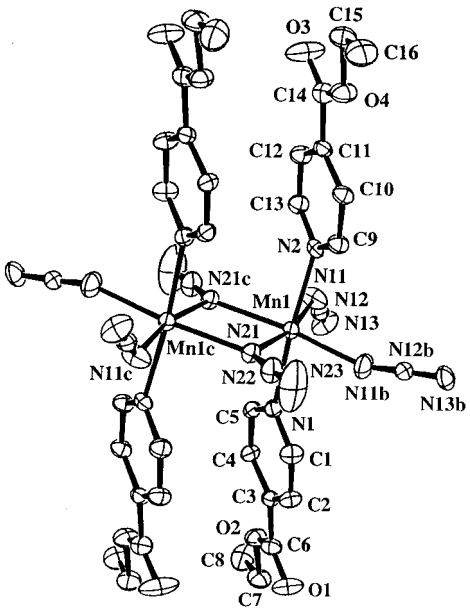

Figure 1. ORTEP drawing (50% of the thermal ellipsoid probability) of $[Mn(Etinc)_2(N_3)_2]_n$ (**2**) with atom labeling scheme.

general schema of four azido end-to-end bridges, linked to the four neighboring manganese atoms and two pyridyl ligands in *trans* arrangement, like compound **1**, but giving, in this case, a 3D compound. The structure shows channels along the solid in which the pyridyl ligands are placed, as can be shown in Figure 3. When the axial ligand has a voluminous group attached to the 4 position, steric hindrance forces the structure to open to a 2D arrangement with the axial ligands placed out of the sheet, as occurs in **1** and **2**. Bond parameters in the bridging region are similar to those found for **1**.

Magnetic Data and Coupling Constants Evaluation. The molar magnetic susceptibilities *vs T* of $[Mn(4\text{-acpy})_2(N_3)_2]_n$ (**1**), $[Mn(Etinc)_2(N_3)_2]_n$ (**2**), and $[Mn(py)_2(N_3)_2]_n$ (**3**) are plotted in Figure 4. In the three cases the χ_M value increases when the temperature decreases, reaching a well-defined maximum at 50.5 K for **1**, 35.0 K for **2**, and 50 K for **3**.

The experimental data for **1** in the range 35−300 K have been fitted to the expression for the quadratic-layer Heisenberg antiferromagnet high-temperature expansion series of Lines[20] derived from $H = \sum_{nn} -JS_iS_j$, where $\sum_{nn}$ runs over all pairs of nearest spins *i* and *j*. The best fit parameters were $J = -3.83(1)$ cm^{-1}, $g = 2.00(0)$, $R = 7.8 \times 10^{-5}$, as was previously reported.[14] The *J* value and the position of the maximum agree with the expression $kT_{max}/|J| = 1.12S(S + 1) + 0.10$, from which a $J = -3.55$ cm^{-1} value is expected.

For compound **2** simultaneous ferro- and antiferromagnetic interactions are expected. The planar M_2N_2 units in which there are two end-on bridging azido ligands with the M−N−M bond angle in the 100−105° range are ferromagnetic for M = Cu, Ni, and Mn, and on the other hand the end-to-end azido bridges give from moderate to strong antiferromagnetic coupling as a function of the bridging bond angles. From the structural data, the behavior of **2** should correspond to ferromagnetic manganese dimeric entities (J_{EO}) coupled antiferromagnetically (J_{EE}) in a quadratic layer. Analytical solution is not available for this topology, but according to the structural data the value of J_{EE} should be close to that found for compound **1** and J_{EO} should also to be close to the value found for the dimeric[12] entity $(\mu_{1,1}\text{-}N_3)_2[Mn(terpy)_2]_2(X)_2$. Therefore, the ferro- and antiferromagnetic interactions may be easily evidenced from the plot of χ_M,

(19) McElearney, J. N.; Balagot, L. L.; Muir, J. A.; Spence, R. D. *Phys. Rev. B* **1979**, *19*, 306.

(20) Lines, M. E. *J. Phys. Chem. Solids* **1970**, *31*, 101.

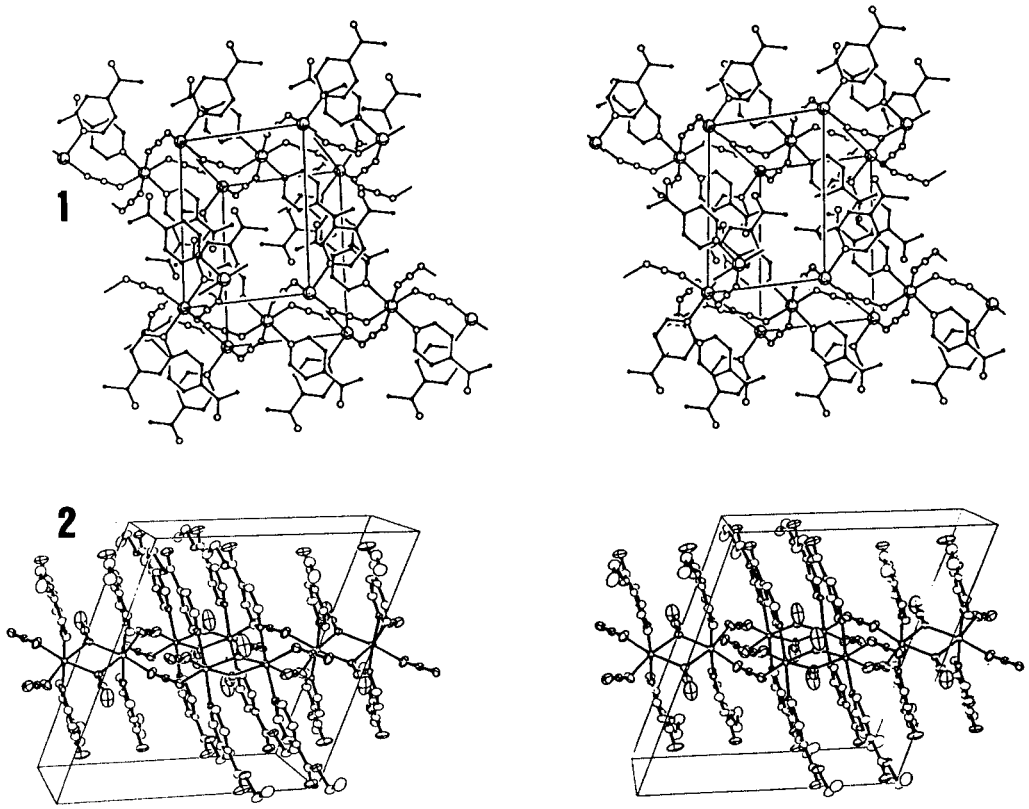

Figure 2. Packing plots of $[Mn(4\text{-acpy})_2(N_3)_2]_n$ (**1**) and $[Mn(Etinc)_2(N_3)_2]_n$ (**2**) showing the four end-to-end azido bridges around each manganese atom for **1**, the four end-to-end azido bridges around each Mn_2N_2 subunit for **2**, and the large intersheet separation due to the 4-acpy or Etinc ligands.

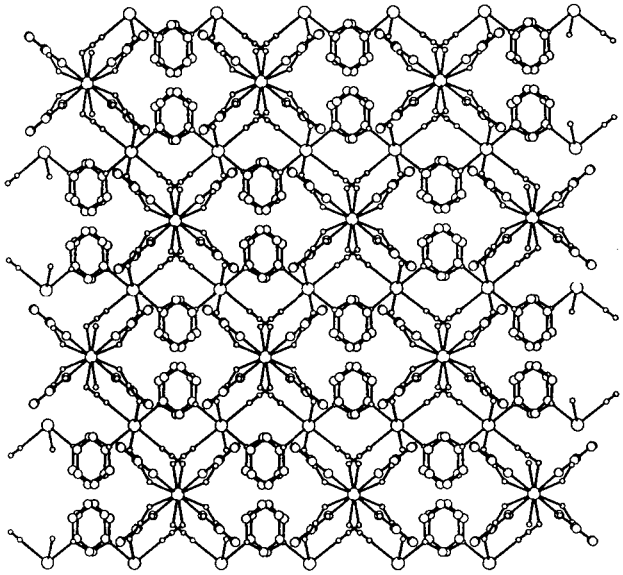

Figure 3. View of the position of the pyridyl ligands for compound **3**. The lower size of the axial ligand in **3** permits the arrangement of the pyridyl rings along channels in the 3D solid.

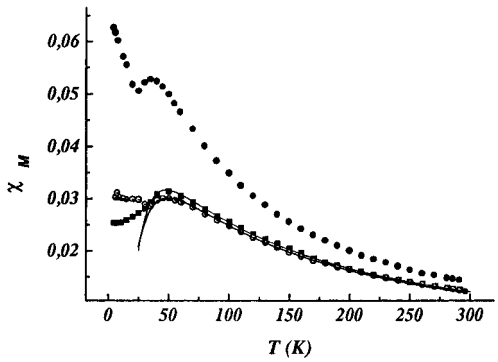

Figure 4. Molar magnetic susceptibility *vs T* plots for **1** (dot center circle), **2** (solid circle), and **3** (solid squares). Solid lines show the best fit obtained for **1** and **3**. (Data recorded at 1.5 T for all of them.)

Figure 4: the maximum of susceptibility indicates that the J_{EE} is not zero and the high values of χ_M in the same range of temperatures show that the ferromagnetic coupling constant J_{EO} is far from negligible.

The experimental data for compound **3** can be fitted with the simple cubic expansion series,[21] although the number of neighboring manganese atoms is 4. The best fit parameters found were $J = -1.35(1)$ cm^{-1}, $g = 2.030(5)$, $R = 5.04 \times 10^{-5}$.

The EPR spectra performed on polycrystalline samples at variable temperature for **1** show that the linewidth of the isotropic signal at $g = 2$ is temperature dependent, peak-to-peak 30 G at room temperature, increasing strongly below 100 K. At 28 K the linewidth is 300 G, and below this temperature the compound becomes silent to EPR. Compound **3** shows similar EPR behavior. This property allows a more precise indication of the ordering temperature which is close to 28 K for **1** and 35 K for **3**. Compound **2** shows a single isotropic signal at $g = 2$, peak-to-peak 46 G at room temperature, 51 G at 77 K, and 80 G at 4 K. The order for **2** is probably not achieved due to the extremely large intersheet distance of 15 Å.

MO Calculations. The superexchange pathway through end-to-end azido bridges between copper or nickel ions has been widely studied during the past few years, and a model was

(21) De Jongh, L. J.; Breed, D. J. *Solid State Commun.* **1974**, *15*, 1061.
(22) Richards, P. M.; Salamon, M. B. *Phys. Rev. B* **1974**, *9*, 32.
(23) Shia, L.; KoKosza, G. *J. Chem. Phys.* **1974**, *60*, 1101.

Scheme 1

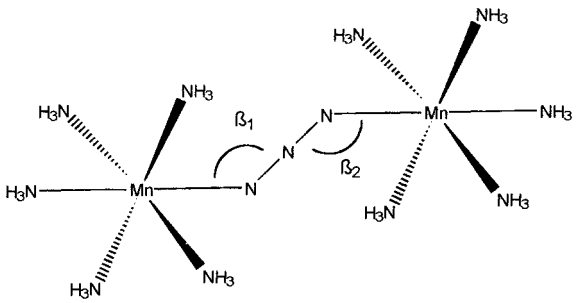

proposed in which the antiferromagnetic component (J_{AF}) of the coupling constant J was successfully correlated with the bond parameters, mainly the Ni−N−N bond angles and the Ni−N−N−N−Ni torsion angle. More recently, this model has been applied to the general pseudohalide end-to-end bridges.[4] This model has been checked for a number of compounds and offers a convenient description of the superexchange pathway and a good approximation to the magnitude of the J values. For the case in which the metallic ions bridged by the pseudohalogen ligands are nickel(II), the magnetically active atomic orbitals are the $d_{x^2-y^2}$ and the d_{z^2}, whereas the filled t_{2g} atomic orbitals remain inactive; in contrast, when the paramagnetic centers are manganese(II), all of the atomic orbitals of the metallic ion are potentially able to offer a more or less effective superexchange pathway. In this work we attempt to extend the model previously checked for the nickel case to the most general case of the manganese(II).

The approach to the problem was similar to that previously reported for the nickel case: MO extended-Hückel calculations were performed by means of the CACAO program,[24] on a dimeric fragment, which models a single end-to-end azido bridge between two manganese ions (Scheme 1).

Calculations were performed by varying the $\beta_1 = \beta_2$ angles in symmetrical form, maintaining the rest of the parameters constant and, on the other hand, varying the Mn−N−N−N−Mn torsion angle, keeping the remainder parameters constant, and taking $\beta_1 = \beta_2 = 120°$. The standard atomic parameters of the CACAO program were used.

For a [MnMn] system, and with the assumption that the Hoffmann relationship[25] between the J_{AF} and the gaps between MOs of the same symmetry, it can be assumed that the magnitude of J_{AF} is a function of $\sum\Delta^2$:

$$\sum\Delta^2 = |E\Phi(x^2 - y^2_{(s)}) - E\Phi(x^2 - y^2_{(a)})|^2 + |E\Phi(z^2_{(s)}) - E\Phi(z^2_{(a)})|^2 + |E\Phi(xy_{(s)}) - E\Phi(xy_{(a)})|^2 + |E\Phi(xz_{(s)}) - E\Phi(xz_{(a)})|^2 + |E\Phi(yz_{(s)}) - E\Phi(yz_{(a)})|^2$$

Taking into account the chosen model, in which d_{z^2} atomic orbitals are always placed in the Mn−N (azido) bond direction, the $d_{x^2-y^2}$ and d_{xy} atomic orbitals always remain orthogonal to the MOs of the bridge and then $|E\Phi(x^2 - y^2_{(s)}) - E\Phi(x^2 - y^2_{(a)})|^2$ and $|E\Phi(xy_{(s)}) - E\Phi(xy_{(a)})|^2$ are always zero. The above expressions are then reduced to the pathways with z component:

$$\sum\Delta^2 = \Delta^2(z^2) + \Delta^2(xz) + \Delta^2(yz)$$

The first step was the calculation of a MO diagram for a fixed $\beta_{1,2} = 120°$ value. The result is shown in Figure 5. Analysis of this diagram indicates that $\Delta^2(x^2 - y^2)$ and $\Delta^2(xy)$

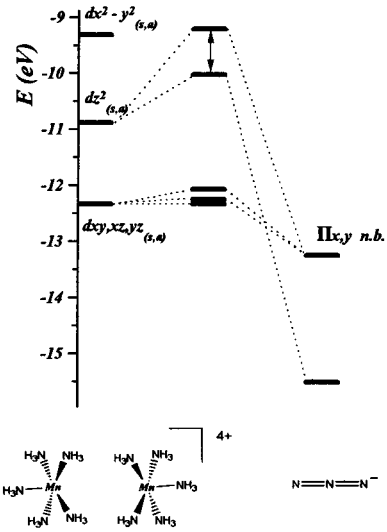

Figure 5. MO diagram for an $[(NH_3)_4-Mn-N-N-N-Mn(NH_3)_4]^{3+}$ system calculated from the parameters Mn−N−N = 120°, Mn−N−N−N−Mn torsion angle = 180°, and the remaining bond parameters indicated in the text. The significant contributions of the azido and the [MnMn] fragments are schematized in the figure.

are zero, as expected, and that the other three possible pathways are effectively active, of which the most effective is the superexchange through the interaction of the d_{z^2} orbitals with the corresponding Π_{xz} MO of the azide bridge, as occurs for copper or nickel ions. The d_{xz} orbitals also interact with Π_{xz}, and most interestingly, the d_{yz} orbitals can interact by means of the Π_{yz} MO of the bridge, which for copper or nickel is orthogonal to the active magnetic orbitals and remains inactive.

The next step was the calculation of a Walsh diagram for the symmetric variation of the $\beta_{1,2}$ values in the range 90−180°, Figure 6. The d_{z^2} interactions were similar to those previously found for the nickel case: $\Delta(z^2)$ show a maximum for $\beta_{1,2} = 110°$, and an accidental orthogonal point was found between 165 and 170°. The $\Delta(xz)$ gap is the maximum for the $\beta_{1,2}$ value of 180° and decreases continuously to zero for $\beta_{1,2} = 90°$ (Figure 6a). $\Delta(yz)$ shows a constant value in all of the $\beta_{1,2}$ range and is independent of the β value. In Figure 6b $\sum\Delta^2$ and their three components are plotted; as occurs for the nickel case, this plot indicates a maximum of the J_{AF} for low Mn−N−N bond angles close to 110° and a minimum of J_{AF} for large Mn−N−N values, close to 160°. Therefore, for the manganese case, J_{AF} is always different from zero.

The study of the torsion angle affords the same qualitative results: the antiferromagnetic interaction should be maximum for a planar arrangement of the manganese ions and the azido bridge and should be minimum for high torsion values, but $\sum\Delta^2$ for torsion 90° is also different from zero, due to the interactions of d_{xz} and d_{yz}, in contrast to the nickel case, for which torsion 90° is an accidental orthogonal point.

The main conclusion derived from this analysis is that an end-to-end azido bridge between two manganese(II) ions should *always* be significantly antiferromagnetic.

The d_{yz} pathway, Figure 7, should also be active for other pseudohalogen bridges, such as cyanate or thiocyanate, and MO calculations for the thiocyanate bridge, modeled according to Scheme 1, and taking the bond lengths as Mn−S = 2.40 Å, S−C = 1.60 Å, C−N = 1.15 Å, and N−Mn = 2.10 Å, are in good agreement with this assumption. This means that as a general trend, the superexchange through the pseudohalide bridges should generally be antiferromagnetic for manganese(II). The above results for the azido bridge are in good agreement with the magnetic behavior of compounds **1** and **3**:

(24) Mealli, C.; Proserpio, D. M. *J. Chem. Educ*. **1990**, *67*, 3399.
(25) Hay, J. P.; Thibeault, J. C.; Hoffmann, R. *J. Am. Chem. Soc*. **1975**, *97*, 4884.

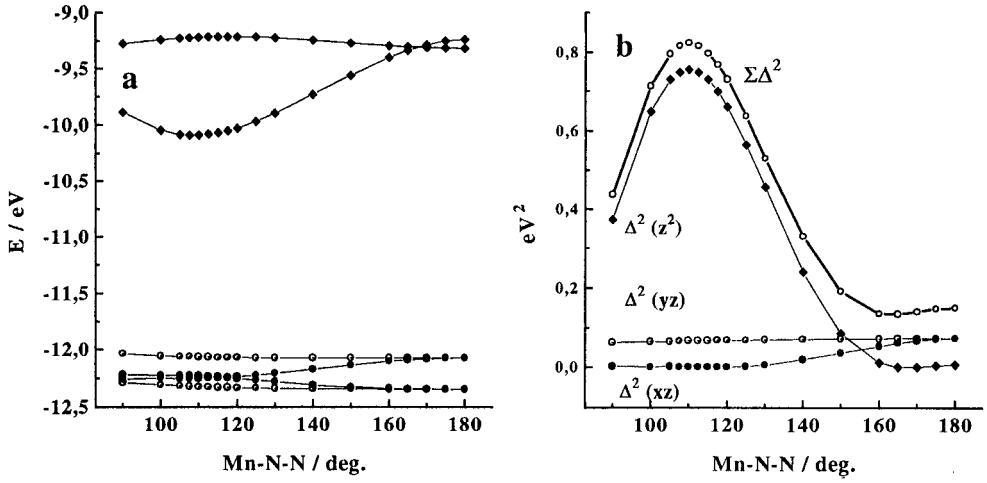

Figure 6. Walsh diagram plots of Δ (a) and $\sum\Delta^2$ (b) *vs* the symmetric variation of the Mn−N−N bond angles, showing the d_{z^2}, d_{xz}, and d_{yz} contributions.

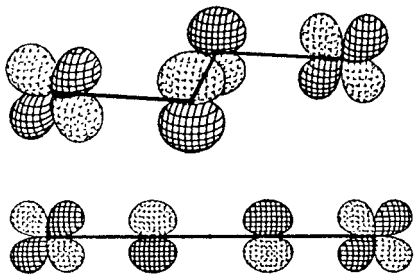

Figure 7. Plot of the $d_{yz(s,a)}$ MO for two extreme Mn−N−N bond angles of 90° and 180° showing the constant overlap and their constant contribution to J_{AF}.

the two compounds show medium Mn−N−N bond angles, but despite the extremely high Mn−N−N−N−Mn torsion angle, the compounds are significantly antiferromagnetic. Nickel compounds with similar torsion angles are effectively noncoupled or show J values lower than -4 cm^{-1}, for a lower number of electrons. On the other hand, the validity of our results can be checked in another way: for copper or nickel(II), for which the Π_{yz} superexchange pathway is not available, when the bridging ligand is thiocyanate, which shows M−N−C bond angles typically close to 170°, the interaction is always *ferromagnetic* as expected.[4] From our conclusions, for the case of the manganese ion the coupling should be *antiferromagnetic*.

The J values obtained for the end-to-end azido bridges are the first reported for the Mn(II)−azido system, and no comparison can be made at present to check our proposal, but in the literature there are reports of some d^5 or d^4 azido or thiocyanate bridged compounds, such as the chromium(II) dimer[26] $(NBu_4)_4[Cr(NCS)_4]_2$ ($J = -8.8$ cm^{-1}), the manganese(III) chains[27] $[Mn(acac)_2(N_3)]_n$ or $[Mn(acac)_2(NCS)]_n$ ($J = -5.3$ and -1.5 cm^{-1}, respectively), the manganese(II) dimer[28] $[Mn_2(tren)_2(NCS)_2](BPh_4)_2$ ($J = -0.2$ cm^{-1}), the two-dimensional $[Mn(EtOH)_2(SCN)_2]_n$ complex,[19] structurally analogous to **1** ($J = -0.6$ cm^{-1}), the manganese(II) chain[29] $[Mn(bipy)(NCS)_2)]_n$ ($J = -2.5$ cm^{-1}), or the manganese(III) $[Mn(salen)(N_3)]_n$ and $[Mn(salen)(NCS)]_n$ chains[30] ($J = -5.4$ and -0.44 cm^{-1}, respectively), which, in agreement with the above conclusions, effectively show antiferromagnetic coupling in all cases.

Acknowledgment. A.E. and R.V. thank the CICYT (Grant PB93/0772) for support of this research. M.A.S.G. acknowledges the financial support of the Kuwait University Research Project SC 077. F.A.M. thanks Prof. C. Kratky (University of Graz) for use of experimental equipment.

Supporting Information Available: Text describing complete crystal data and tables listing anisotropic thermal parameters, atom coordinates, angles, and distances for compound **2** (7 pages). Ordering information is given on any current masthead page.

IC9603464

(26) Larkworthy, L. F.; Leonard, G. A.; Povey, D. C.; Tandon, S. S.; Tucker, B. J.; Smith, G. W. *J. Chem. Soc., Dalton Trans.* **1994**, 1425.
(27) Gregson, A. K.; Moxon, N. T. *Inorg. Chem.* **1982**, *21*, 586.
(28) Laskowski, E. J.; Hendrickson, D. N. *Inorg. Chem.* **1978**, *2*, 457.
(29) Dockum, B. W.; Eisman, G. A.; Witten, E. H.; Reiff, W. M. *Inorg. Chem.* **1982**, *22*, 150.
(30) Kennedy, B. J.; Murray, K. S. *Inorg. Chem.* **1985**, *24*, 1552.